Biogeosciences Discuss., 3, 1313–1354, 2006
www.biogeosciences-discuss.net/3/1313/2006/


Biogeosciences Discussions

*Biogeosciences Discussions* is the access reviewed discussion forum of *Biogeosciences*

# Marine geochemical data assimilation in an efficient Earth System Model of global biogeochemical cycling

**A. Ridgwell[1], J. C. Hargreaves[2], N. R. Edwards[3], J. D. Annan[2], T. M. Lenton[4], R. Marsh[5], A. Yool[5], and A. Watson[4]**

[1]Department of Earth and Ocean Sciences, University of British Columbia, Vancouver, BC, USA
[2]Frontier Research Center for Global Change, 3173-25 Showa-machi, Kanazawa-ku, Yokohama, Kanagawa 236-0001, Japan
[3]Earth Sciences, The Open University, Walton Hall, Milton Keynes, UK
[4]School of Environmental Sciences, University of East Anglia, Norwich, UK
[5]National Oceanography Centre, Southampton, European Way, Southampton SO14 3ZH, UK

Received: 17 July 2006 – Accepted: 1 August 2006 – Published: 10 August 2006

Correspondence to: A. Ridgwell (andy@seao2.org)

## Abstract

We have extended the 3-D ocean based "Grid ENabled Integrated Earth system model" (GENIE-1) to help understand the role of ocean biogeochemistry and marine sediments in the "long-term" (~100 to 100 000 year) regulation of atmospheric $CO_2$, and the importance of feedbacks between $CO_2$ and climate. Here we describe the ocean carbon cycle, which is based around a simple single nutrient (phosphate) control on biological productivity. The addition of ocean-sediment interactions is presented elsewhere (Ridgwell and Hargreaves, 2006[1]).

We have calibrated the model parameters controlling ocean carbon cycling in GENIE-1 by assimilating 3-D observational datasets of phosphate and alkalinity using an ensemble Kalman filter method. The calibrated (mean) model predicts a global export production of particulate organic carbon (POC) of 8.9 PgC $yr^{-1}$, and reproduces the main features of dissolved oxygen distributions in the ocean. For estimating biogenic calcium carbonate ($CaCO_3$) production, we have devised a parameterization in which the $CaCO_3$:POC export ratio is related directly to ambient saturation state. Calibrated global $CaCO_3$ export production (1.2 PgC $yr^{-1}$) is close to recent marine carbonate budget estimates.

The GENIE-1 Earth system model is capable of simulating a wide variety of dissolved and isotopic species of relevance to the study of modern global biogeochemical cycles as well as past global environmental changes recorded in paleoceanographic proxies. Importantly, even with 12 active biogeochemical tracers in the ocean and including the calculation of feedbacks between atmospheric $CO_2$ and climate, we achieve better than 1000 years per (2.4 GHz) CPU hour on a desktop PC. The GENIE-1 model thus provides a viable alternative to box and zonally-averaged models for studying global biogeochemical cycling over all but the very longest (>1 000 000 years) time-scales.


[1] Ridgwell, A. and Hargreaves, J. C.: An efficient Earth System Model of Global biogeochemical cycling (II) Regulation of atmospheric $CO_2$ by deep-sea sediments, Global Biogeochem. Cycles, submitted, http://www.seao2.org/pubs/ridgwell_hargreaves_manuscript.pdf.



BGD

3, 1313–1354, 2006

## 1 Introduction

The societal importance of better understanding the role of the ocean in regulating atmospheric $CO_2$ (and climate) is unquestionable. Reorganizations of ocean circulation and nutrient cycling as well as changes in biological productivity and surface temperatures all modulate the concentration of $CO_2$ in the atmosphere, and are likely central to explaining the observed variability in $CO_2$ over the glacial-interglacial cycles of the past ~800 000 years (Siegenthaler et al., 2005). These same marine carbon cycle processes will also affect the uptake of fossil fuel $CO_2$ in the future. Interactions between marine biogeochemistry and deep-sea sediments together with imbalances induced between terrestrial weathering and the sedimentary burial of calcium carbonate ($CaCO_3$) exert further controls on atmospheric $CO_2$ (Archer et al., 1998). These sedimentation and weathering processes are suspected to have dominated the recovery of the Earth system from catastrophic $CO_2$ release in the geological past (Zachos et al., 2005), and will largely determine the long-term (>1000 year) future fate of fossil fuel $CO_2$ (Archer et al., 1998).

Quantifying the behavior of atmospheric $CO_2$ is complicated by the fact that $CO_2$ exerts (via the radiative forcing of climate) an influence on marine biogeochemical cycles. For instance, anthropogenically-driven increases in atmospheric $CO_2$ will be amplified because $CO_2$ solubility decreases at higher temperature and as a result of thermally (and/or fresh water) induced changes in ocean stratification and transport (Plattner et al., 2001; Sarmiento et al., 1998). Understanding how atmospheric $CO_2$ is regulated thus necessarily requires feedbacks between $CO_2$ and climate to be taken into account. Coupled GCM ocean-atmosphere plus carbon cycle models (e.g., "HadCM3LC", Cox et al., 2000) are important tools for assessing climate change and associated feedbacks over the next few hundred years. However, their computational demands currently make them unsuitable for investigating time-scales beyond 1000 years or for conducting sensitivity studies. So-called "off-line" carbon cycle models in which the ocean circulation has been pre-calculated (such as the off-line tracer transport HAMOCC3



BGD
3, 1313–1354, 2006



EGU

model of Maier-Reimer, 1993) are much faster. However, the fixed circulation field employed in these models means that the importance of feedbacks with climate cannot easily be explored, except in a highly parameterized manner (Archer et al., 2004; Archer, 2005).

In contrast, marine biogeochemical box models, which consider the global ocean in terms of relatively few (typically between about 3 and about 12) distinct volumes (the "boxes"), are extremely computationally efficient. Models of this type have an illustrious pedigree (e.g., Broecker and Peng, 1986; Sarmiento and Toggweiler, 1984) and continue today to be the tools of choice for many questions involving processes operating on ~10 000 years or longer time-scales. For instance, when ocean-sediment interactions and weathering feedbacks are important (e.g., Ridgwell, 2005; Yool and Tyrrell, 2005; Zeebe and Westbroek, 2003) or where the inherent uncertainties are large and need to be extensively explored (e.g., Parekh et al., 2004). Box models, as with GCMs, have specific limitations. Validation against marine observations and sediment records is problematic because large volumes of the ocean are homogenized in creating each "box", whereas biogeochemical processes are extremely heterogeneous both within ocean basins as well as between them. It is also difficult to incorporate a responsive climate or circulation, which is why almost all box models are in effect offline tracer transport models (the coupled meridional box model of Gildor et al., 2002 being one exception). Concerns have also been recently raised regarding whether box models present an inherently biased picture of certain aspects of the oceanic control of atmospheric $CO_2$ (Archer et al., 2003).

This has led to the development of fast climate models with reduced spatial resolution and/or more highly parameterized "physics" – known variously as Earth System (Climate) Models (ESMs) (Weaver et al., 2001) and Earth System Models of Intermediate Complexity (EMICs) (Claussen et al., 2002). While ESMs have been instrumental in helping address a range of carbon cycling and climate change questions, we believe that they have yet to realize their full potential. In particular, simulations on the time-scale of ocean-sediment interaction (order 10 000 years) are still relatively com-

putationally expensive in many ESMs based around 3-D ocean circulation models, whereas in faster "2.5-D" models (e.g., Marchal et al., 1998) the zonal averaging of the basins complicates comparison between model and paleoceanographic data (Ridgwell, 2001).

In this paper we present a representation of marine biogeochemical cycling within a 3-D ocean based Earth system model, which we calibrate for the modern carbon cycle via a novel assimilation of marine geochemical data. In a companion paper (Ridgwell and Hargreaves, 2006[1]) we describe the addition of sedimentary diagenesis and carbonate burial in the deep sea. Together, these developments allow us to explore important questions surrounding future fossil fuel $CO_2$ uptake by the ocean and including the role of major feedbacks with climate (described elsewhere, Ridgwell and Hargreaves, 2006[1]; Ridgwell et al., 2006[2]).

This paper is laid out as follows; we first describe the ocean biogeochemistry model itself (Sect. 2), then how the model is calibrated by assimilation observed marine geochemical data (Sect. 3). In Sect. 4 we present the predictions of the model for modern ocean biogeochemical cycling, and discuss the implications for exceptionally low resolution 3-D ocean circulation models. We conclude in Sect. 5.

## 2 Description of the "GENIE-1" model

The basis of our work is the fast climate model of Edwards and Marsh (2005) ("C-GOLDSTEIN"), which features a reduced physics (frictional geostrophic) 3-D ocean circulation model coupled to a 2-D energy-moisture balance model (EMBM) of the atmosphere and a dynamic-thermodynamic sea-ice model (see Edwards and Marsh, 2005 for a full description). The ocean model used here is non-seasonally forced and implemented on a 36×36 equal-area horizontal grid, comprising 10° increments

[2] Ridgwell, A., Zondervan, I., Hargreaves, J. C., Bijma, J., and Lenton, T. M.: Significant long-term increase of fossil fuel $CO_2$ uptake from reduced marine calcification, Nature, submitted, http://www.seao2.org/pubs/ridgwelletalb_manuscript.pdf, 2006.

in longitude but uniform in sine of latitude, giving ~3.2° latitudinal increments at the equator increasing to 19.2° in the highest latitude band. The ocean has 8 $z$-coordinate levels in the vertical. The grid and bathymetry is shown in Fig. 1.

Along with temperature and salinity, the oceanic concentrations of "biogeochemical" tracers are advected, diffused, and convected on-line by the ocean circulation model. To enable a broad range of questions concerning global biogeochemical cycling to be addressed, the GENIE-1 model contains the definitions of 39 dissolved tracers and isotopic properties relevant to future global change and paleoceanography, as well as their relationships (if any) to sedimentary solids and atmospheric gases. For this present study, we select only; total dissolved inorganic carbon (DIC), alkalinity (ALK), phosphate ($PO_4$), oxygen ($O_2$), CFC-11 and CFC-12, the carbon and phosphorus components of dissolved organic matter, plus the stable ($^{13}C$) and radio- ($^{14}C$) isotope abundances associated with both DIC and dissolved organic carbon. The circulation model thus acts on the 3-D spatial distribution of a total of 14 tracers (including temperature and salinity).

As with many ocean circulation models, C-GOLDSTEIN employs a rigid lid surface boundary condition (i.e., grid cell volumes are not allowed to change). Net precipitation-minus-evaporation (P-E) at the ocean surface is then implemented as a virtual salinity flux rather than an actual loss or gain of freshwater. The concentration of biogeochemical tracers (DIC, ALK, $PO_4$, etc) should respond similarly to salinity; becoming more concentrated or dilute depending on the sign of P-E. To achieve this, one could apply virtual fluxes of the biogeochemical tracers along with salinity to the ocean surface (e.g., see the OCMIP-2 protocol; Najjar and Orr, 1999). We take the alternative approach here, and salinity-normalize the biogeochemical tracer concentration field prior to the calculation of ocean transport (Marchal et al., 1998).

We have developed a representation of marine biogeochemical cycling called BIOGEM (for; BIOGEochemical Model) that calculates the redistribution of tracer concentrations occurring other than by transport by the circulation of the ocean. This happens through the removal from solution of nutrients ($PO_4$) together with DIC and ALK, by



BGD
3, 1313–1354, 2006



EGU

biological activity in the sunlit surface ocean layer (the "euphotic zone", which has a depth of $h_e$=175 m in the 8-level ocean model configuration). The resulting export of particulate matter to the ocean interior is subject to "remineralization" – the metabolic and dissolution processes that release constituent species back into inorganic solution (but at greater depth). Further redistribution of tracers occurs through gas exchange with the atmosphere as well as due to the creation and destruction of dissolved organic matter. BIOGEM has a conceptual relationship with the climate model as shown schematically in Fig. 2. We refer to the overall composite model as GENIE-1.

We carry out the biogeochemical manipulation of tracer concentration fields asynchronously to maximize overall model speed. In this study, BIOGEM is called once every 5 time-steps taken by the ocean circulation model (i.e., 5×0.01 yr=0.05 yr). We find no discernable impact of this decoupling compared to carrying out the same time step length as the ocean (0.01 yr), even in response to rather extreme (15 000 PgC) releases of (fossil fuel) $CO_2$ to the atmosphere.

### 2.1 Ocean biogeochemical cycling

The low vertical resolution of the ocean circulation model and need to maximize computational speed (for long simulations) dictates that the "biological" part of the marine carbon cycle be relatively abstracted. We estimate new (export) production directly from available surface nutrient concentrations, a tactic used in many ocean carbon cycle models. In other words, what we have is "conceptually not a model of biology in the ocean but rather a model of biogenically induced chemical fluxes (from the surface ocean)" (Maier-Reimer, 1993). Overall, the scheme is functionally similar to that of Parekh et al. (2005), and we adopt their notation where relevant. The main difference is that we currently consider only a single nutrient, phosphate ($PO_4$), rather than co-limitation with iron (Fe).

The governing equations in BIOGEM for the changes in phosphate and dissolved organic phosphorus (DOP) concentrations occurring in the surface ocean layer (but omitting the extra transport terms that are calculated by the ocean circulation model;

Edwards and Marsh, 2005) are;

$$\frac{\partial \mathrm{PO_4}}{\partial t} = -\Gamma + \lambda \mathrm{DOP} \quad (1)$$

$$\frac{\partial \mathrm{DOP}}{\partial t} = \nu\Gamma - \lambda \mathrm{DOP} \quad (2)$$

$$\Gamma = u_0^{\mathrm{PO_4}} \cdot \frac{\mathrm{PO_4}}{\mathrm{PO_4} + K^{\mathrm{PO_4}}} \cdot (1 - A) \cdot \frac{I}{I_0} \quad (3)$$

where $\Gamma$ is the biological uptake of $PO_4$. $\Gamma$ is calculated from; (i) an assumed maximum uptake rate of phosphate (mol $PO_4\,kg^{-1}\,yr^{-1}$) that would occur in the absence of any limitation on phytoplankton growth, and (ii) a Michaelis-Menten type kinetic limitation of nutrient uptake, of which $K^{PO_4}$ is the half-saturation constant. Because of the degree of abstraction of ecosystem function inherent in our model, what the appropriate values for either $u_0^{PO_4}$ or $K^{PO_4}$ are not obvious, and so are subsequently calibrated (see Sect. 3 and Table 1). We apply two modifiers on productivity representing the effects of sub-optimal ambient light levels and the fractional sea ice coverage of each grid cell ($A$) (Edwards and Marsh, 2005). A full treatment of the effects of light limitation on phytoplankton growth is beyond the scope of the current model. The strength of local insolation ($I$) is therefore simply normalized to the solar constant ($I_0$) to give a limitation term that is linear in annual incident insolation. A proportion ($\nu$) of $PO_4$ taken up by the biota is partitioned into dissolved organic phosphorus (DOP). The relatively labile dissolved organic molecules are subsequently remineralization with a time constant of $1/\lambda$. The values of $\nu$ and $\lambda$ are assigned following the assumptions of the OCMIP-2 protocol (Najjar and Orr, 1999); $\nu$=0.66 and $\lambda$=0.5 $yr^{-1}$.

The particulate organic matter fraction is exported vertically (and without lateral advection) out of the surface ocean layer at the next model time-step. Because there is no explicit standing plankton biomass in the model, the export flux of particulate organic



BGD
3, 1313–1354, 2006



EGU

phosphorus ($F^{POP}_{z=h_e}$, in units of mol $PO_4\,m^{-2}\,yr^{-1}$) is equated directly with $PO_4$ uptake (Eq. 1);

$$F^{POP}_{z=h_e} = \int_{h_e}^{0} \rho \cdot (1 - v) \cdot \Gamma \, dz \tag{4}$$

where $\rho$ is the density of seawater and $h_e$ the thickness of the euphotic zone (175 m in the 8-level version of this ocean model).

In the production of organic matter, dissolved inorganic carbon (DIC) is taken out of solution in a 106:1 molar ratio with $PO_4$ (Redfield et al., 1963) while $O_2$ takes a −170:1 ratio with $PO_4$ (Anderson and Sarmiento, 1994). The effect on total alkalinity (ALK) of the biological uptake and remineralization of nitrate ($NO_3$) is accounted for via a modification of ALK in a −1:1 ratio with the quantity of $NO_3$ transformed. Because we do not model the nitrogen cycle explicitly in this paper, we link ALK directly to $PO_4$ uptake and remineralization through the canonical 16:1 N:P ratio (Redfield et al., 1963). For convenience, we will describe the various transformations involving organic matter in terms of carbon (rather than phosphorus) units, the relationship between organic matter export fluxes being simply;

$$F^{POC}_{z=h_e} = 106 \cdot F^{POP}_{z=h_e} \tag{5}$$

We represent the remineralization of particulate organic carbon (POC) as a process occurring instantaneously throughout the water column. We partition POC into two distinct fractions with different fates in the water column, following Ridgwell (2001) but adopting an exponential decay as an alternative to a power law. The POC flux at depth $z$ in the water column is;

$$F^{POC}_{z} = F^{POC}_{z=h_e} \cdot \left( \left(1 - r^{POC}\right) + r^{POC} \cdot \exp\left( \frac{z_{h_e} - z}{l^{POC}} \right) \right) \tag{6}$$

The parameters; $l^{POC}$ (the length-scale) and $r^{POC}$ (the initial partitioning of POC into a labile fraction) are calibrated (Table 1). Because we explicitly resolve the individual "components" (i.e., C, $^{13}C$, P, ...) of organic matter, the GENIE-1 model can be

used to quantify the effect of fractionation between the components of organic matter during remineralization (e.g., Shaffer et al., 1999) as well as between different carbon isotopes. However, we assume no fractionation during remineralization in this present study. The residual flux of particulate organic material escaping remineralization within the water column is remineralized at the ocean floor, making the ocean-atmosphere system "closed" (i.e., there is no loss or gain to the system) with respect to these tracers.

The modern ocean is oxic everywhere at the resolution of our model (e.g., see Fig. 6). In an ideal model, remineralization would not deplete dissolved oxygen below zero anywhere in the ocean. However, $O_2$ availability may be insufficient under different (past) ocean circulation regimes and continental configurations. To broaden the applicability of the GENIE-1 model to past climates and biogeochemical cycling, we limit remineralization according to the total availability of electron acceptors – if dissolved $O_2$ is depleted and $NO_3$ is selected as an active tracer in the model, denitrification occurs to provide the necessary oxidant; $2NO_3^- \rightarrow N_2 + 3O_2$. If $NO_3^-$ becomes depleted and $SO_4^{2-}$ has been selected as an active tracer, sulphate reduction occurs; $2H^+ + SO_4^{2-} \rightarrow H_2S + 2O_2$. If the total concentration of selected electron-accepting tracer species ($O_2$, $NO_3$, $SO_4$) is still insufficient, remineralization of POC is restricted. Our strategy thus differs from other modeling approaches in which remineralization always strictly conforms to a predetermined profile and the consequences of excess oxidation over $O_2$ availability are resolved either by numerically preventing negative oxygen concentrations occurring (e.g. Zhang et al., 2001, 2003), or by allowing the tracer transport of negative $O_2$ concentrations (e.g., Hotinski et al., 2001). (We treat the remineralization of dissolved organic matter in an analogous manner if $O_2$ availability is insufficient.) $H_2S$ created through sulphate reduction is oxidized in the presence of $O_2$ at a rate (mM $H_2S$ $h^{-1}$);

$$\frac{d[H_2S]}{dt} = k \cdot [H_2S] \cdot [O_2]^2 \quad (7)$$

where $[H_2S]$ and $[O_2]$ are the dissolved concentrations of hydrogen sulphide and oxygen, respectively, and $k=0.625\,mM^{-2}\,h^{-1}$ (Zhang and Millero, 1993).

Open ocean dwelling calcifying plankton such as coccolithophorids and foraminifera produce calcium carbonate ($CaCO_3$) in addition to organic compounds (see Ridgwell and Zeebe, 2005 for a review of the global carbonate cycle). As the ecological processes which regulate calcifier activity are not well understood, early models incorporating marine carbonate production calculated the export flux of $CaCO_3$ in a fixed production ratio with POC (e.g., Broecker and Peng, 1986; Yamanaka and Tajika, 1996). Derivatives of this approach modify the $CaCO_3$:POC rain ratio as some function of temperature (e.g., Marchal et al., 1998) and/or opal flux (e.g., Archer et al., 2000; Heinze et al., 1999; Heinze, 2004). Current ecosystem models include a measure of competition between calcifying phytoplankton such as coccolithophores and non-calcifying ones such as diatoms to estimate $CaCO_3$ production (e.g., Bopp et al., 2003; Moore et al., 2002). However, there are drawbacks with this strategy because there are doubts as to whether autotrophic coccolithophorids are the dominant source of $CaCO_3$ in the open ocean (Schiebel, 2002), or whether *Emiliania huxleyi* is a sufficiently representative species of global coccolith carbonate production to be chosen as the "functional type" calcifying species in ecosystem models.

Recent work has introduced a further dimension as to how $CaCO_3$ production should be represented in models. Experiments have shown that planktic calcifiers such as coccolithophores (Delille et al., 2005; Riebesell et al., 2000; Zondervan et al., 2001) and foramifera (Bijma et al., 1999) produce less carbonate at lower ambient carbonate ion concentrations ($CO_3^{2-}$). A progressive reduction in surface $CO_3^{2-}$ is an expected consequence of fossil fuel invasion into the ocean (Caldeira and Wickett, 2003; Freely et al., 2004; Kleypas et al., 1999; Orr et al., 2005). Several recent studies have incorporated a response of the $CaCO_3$:POC rain ratio to changes in surface ocean carbonate chemistry, by employing a parameterization based on the deviation from modern surface ocean conditions of either $CO_2$ partial pressure (Heinze, 2004) or $CO_3^{2-}$ (Barker et al., 2003). We present a new approach here, one which relates the export flux of

$CaCO_3$ ($F_{z=h_e}^{CaCO_3}$) to the POC flux ($F_{z=h_e}^{POC}$) via a thermodynamically-based description of carbonate precipitation rate;

$$F_{z=h_e}^{CaCO_3} = \gamma \cdot r_0^{CaCO_3:POC} \cdot F_{z=h_e}^{POC} \quad (8)$$

where $r_0^{CaCO_3:POC}$ is a spatially-uniform scalar, and $\gamma$ is a thermodynamically-based local modifier of the rate of carbonate production (and thus of the $CaCO_3$:POC rain ratio), defined;

$$\gamma = (\Omega - 1)^{\eta} \qquad \Omega > 1.0 \quad (9a)$$

$$\gamma = 0.0 \qquad \Omega \leq 1.0 \quad (9b)$$

where $\eta$ is a constant and $\Omega$ is the ambient surface saturation state (or "solubility ratio") with respect to calcite, defined by the ratio of the product of calcium ion ($Ca^{2+}$) and carbonate ion ($CO_3^{2-}$) concentrations to $K_{SP}$, the solubility constant (Zeebe and Wolf-Gladrow, 2001);

$$\Omega = \frac{[Ca^{2+}][CO_3^{2-}]}{K_{SP}} \quad (10)$$

In formulating this parameterization we have drawn on descriptions of abiotic carbonate system dynamics in which the experimentally observed precipitation rate can be linked to saturation via an equation with the same form as Eq. (8) (e.g., Burton and Walter, 1987). What this equation says is that the precipitation rate increases with a greater ambient environmental degree of supersaturation with respect to the solid carbonate phase ($\Omega$>1.0), with the power parameter $\eta$ controling how non-linear the response of calcification is. At ambient saturation states below the point of thermodynamic equilibrium ($\Omega$=1.0) ("undersaturation") no carbonate production occurs. It should be noted that although coccolithophorid and foraminiferal calcification rates are observed to respond to changes in saturation (e.g., Bijma et al., 1999; Delille et al., 2005; Riebesell et

al., 2000; Zondervan et al., 2001), we do not explicitly capture other important controls. Instead, we have implicitly collapsed the (poorly understood) ecological and physical oceanographic controls on carbonate production onto a single, purely thermodynamic dependence on Ω.

For this paper we take our prior assumptions regarding the suspected values of $\eta$ (Table 1) from previous analysis of neritic (shallow water) calcification (Langdon and Atkinson, 2005; Opdyke and Wilkinson, 1993; Ridgwell, 2004; Zeebe and Westbroek, 2003). Elsewhere, we collate available observational data on pelagic calcifiers and explore the effect of alternative prior assumptions in $\eta$.

The remineralization (dissolution) of $CaCO_3$ in the water column is treated in a similar manner to particulate organic carbon (the parameter nomenclature being analogous to Eq. 6);

$$F_z^{CaCO_3} = F_{z=h_e}^{CaCO_3} \cdot \left( \left(1 - r^{CaCO_3}\right) + r^{CaCO_3} \cdot \exp\left( \frac{z_{h_e} - z}{l^{CaCO_3}} \right) \right) \quad (11)$$

The values of $r^{CaCO_3}$ and $l^{CaCO_3}$ are also calibrated (Table 1). With the GENIE-1 model configured without a coupled sediment model as here, all $CaCO_3$ reaching the ocean floor is dissolved.

## 2.2 Air-sea gas exchange

The flux of gases ($mol\,m^{-2}\,yr^{-1}$) across the air-sea interface is given by;

$$F = k \cdot \rho \cdot (C_w - \alpha \cdot C_a) \cdot (1 - A) \quad (12)$$

where $k$ is the gas transfer velocity ($m\,yr^{-1}$), $\rho$ the density of sea-water ($kg\,m^{-3}$), $C_w$ the concentration of the gas dissolved in the surface ocean ($mol\,kg^{-1}$), $\alpha$ is the solubility coefficient ($mol\,kg^{-1}\,atm^{-1}$) (calculated from the coefficients listed by Wanninkhof (1992), and references therein), $C_a$ the concentration of the gas in the overlying atmosphere (atm), and $A$ the fractional ice-covered area. Gas transfer velocities are



BGD
3, 1313–1354, 2006



EGU

calculated as a function of wind speed following Wanninkhof (1992);

$$k = a \cdot u^2 \cdot \left(Sc/660\right)^{-0.5} \quad (13)$$

where $u$ is the annual mean climatological wind speed and $Sc$ is the Schmidt Number for the specific gas following Wanninkhof (1992) (and references therein). We use the scalar annual average wind speed field of Trenberth et al. (1989) for calculating air-sea gas exchange and set the scaling constant $a$=0.31 (Wanninkhof, 1992), which gives us a global annual mean gas transfer coefficient for $CO_2$ equal to 0.058 mol m$^{-2}$ yr$^{-1}$ $\mu$atm$^{-1}$ in the calibrated model (Sect. 3.2).

For completeness, we include the parameterization of air-sea gas exchange for all the gases listed by Wanninkhof (1992) (the calculation is not made if the corresponding dissolved tracer in the ocean is not selected). To facilitate analysis of the biogeochemical consequences of extreme anoxia in the geologic past, we also allow for the exchange of $H_2S$, for which we take the solubility following Millero (1986) and Schmidt number from Khalil and Rasmussen (1998).

### 2.3 Isotopic tracers and fractionation

Fractionation occurs between $^{12}C$ and $^{13}C$ during the biological fixation of dissolved carbon (as $CO_{2(aq)}$) to form organic and inorganic (carbonate) carbon, as well as during air-sea gas exchange. For the production of organic carbon (both as POC and DOC) we adopt the fractionation scheme of Ridgwell (2001);

$$\delta^{13}C^{POC} = \delta^{13}C^{CO_{2(aq)}} - \varepsilon_f + (\varepsilon_f - \varepsilon_d) \cdot \frac{K_Q}{[CO_{2(aq)}]} \quad (14)$$

where $\delta^{13}C^{CO_{2(aq)}}$ and $[CO_{2(aq)}]$ are the isotopic composition and concentration of $CO_{2(aq)}$, respectively. $\varepsilon_f$ and $\varepsilon_d$ are fractionation factors associated with enzymic intercellular carbon fixation and $CO_{2(aq)}$ diffusion, respectively, and assigned values of

$\varepsilon_f$ =25 and $\varepsilon_d$ =0.7 (Rau et al., 1996, 1997). $K_Q$ is an empirical approximation of the model of Rau et al. (1996, 1997) as described by Ridgwell (2001);

$$K_Q^{=} 2.829 \times 10^{-10} - 1.788 \times 10^{-7} \cdot T + 3.170 \times 10^{-5} \cdot T^2 \quad (15)$$

with $T$ the ocean temperature in Kelvin.

For $CaCO_3$, we adopt a temperature-dependent fractionation for calcite following Mook (1986). The air-sea $^{13}C/^{12}C$ fractionation scheme follows that of Marchal et al. (1998), with the individual fractionation factors all taken from Zhang et al. (1995).

For radiocarbon, the $^{14}C/^{12}C$ fractionation factors are simply the square of the factors calculated for $^{13}C/^{12}C$ at every step. Radiocarbon abundance also decays with a half-life of 5730 years (Stuiver and Polach, 1977). We report radiocarbon isotopic properties in the $\Delta^{14}C$ notation, which we calculate directly from model-simulated $\delta^{13}C$ and $\delta^{14}C$ values by;

$$\Delta^{14}C = 1000 \cdot \left( \left( 1 + \frac{\delta^{14}C}{1000} \right) \cdot \frac{0.975^2}{\left( 1 + \frac{\delta^{13}C}{1000} \right)^2} - 1 \right) \quad (16)$$

which is the exact form of the more commonly used approximation; $\Delta^{14}C = \delta^{14}C - 2 \cdot \left( \delta^{13}C + 25 \right) \cdot \left( 1 + \delta^{14}C/1000 \right)$ (Stuiver and Polach, 1977). $\delta^{14}C$ is calculated using $\delta^{14}C = (A_S/A_{abs} - 1) \cdot 1000$, where $A_S$ is the (model-simulated) sample activity and $A_{abs}$ is the absolute international standard activity, related to the activity of the oxalic acid standard ($A_{Ox}$) by $A_{abs} = 0.95 \cdot A_{Ox}$. $A_{Ox}$ is assigned a ratio of $1.176 \times 10^{-12}$ (Key et al., 2004).

## 2.4 Definition of the aqueous carbonate system

We define alkalinity following Dickson (1981) but excluding the effect of $NH_3$, $HS^-$, and $S^{2-}$. The set of carbonate dissociation constants are those of Mehrbach et al. (1973),

as refitted by Dickson and Millero (1987), with *p*H calculated on the seawater *p*H scale (pHSWS). Numerical solution of the system is via an implicit iterative method, seeded with the hydrogen ion concentration ($[H^+]$) calculated from the previous time-step (Ridgwell, 2001) (or with $10^{-7.8}$ from a "cold" start). We judge the system to be sufficiently converged when $[H^+]$ changes by less than 0.1% between iterations. This brings *p*H and $fCO_2$ to within ±0.001 units (pHSWS) and ±0.2 $\mu$atm, respectively, compared to calculations made using the model of Lewis and Wallace (1998).

Dissolved calcium, total boric acid, sulphate, and fluorine can all be selected as prognostic tracers in the ocean biogeochemistry model and their oceanic distributions simulated explicitly. Here, we do not select them, and instead estimate their concentrations from salinity (Millero, 1982, 1995) in order to solve the aqueous carbonate system. Furthermore, because we do not consider the marine cycling of silicic acid ($H_4SiO_4$) here we implicitly assume a zero concentration everywhere. The error in atmospheric $CO_2$ induced by this simplification compared to observed concentrations (Conkright et al., 2002) is <1 $\mu$atm.

## 3 Data assimilation and "calibration" of the marine carbon cycle

The degree of spatial and temporal abstraction inherent in representations of complex global biogeochemical processes inevitably gives rise to important parameters whose values are not well known a priori. Because of the computational cost of most 3-D ocean biogeochemical models, calibration of the poorly known parameters usually proceeds by trial-and-error with the aid of limited sensitivity analysis. The relative speed of the GENIE-1 model allows us to explore a new efficient and optimal approach to this problem by assimilating 3-D fields of marine geochemical data using a version of the ensemble Kalman filter which has been developed to simultaneously estimate multiple parameters in climate models.

### 3.1 EnKF methodology

The model parameters were optimized with respect to 3-D data fields that are available for the present day climatological distributions of phosphate ($PO_4$) (Conkright et al., 2002) and alkalinity (ALK) (Key et al., 2004) in the ocean. The data were assimilated into the model using an iterative application of the ensemble Kalman filter (EnKF), which is described more fully in Annan et al. (2005a, b). The EnKF was originally introduced as a state estimation algorithm (Evensen, 1994). We introduce the parameters into the analysis simply by augmenting the model state with them. The EnKF solves the Kalman equation for optimal linear estimation by using the ensemble statistics to define the mean and covariance of the model's probability distribution function. In other words, the resulting ensemble members are random samples from this probability distribution function. Although this method is only formally optimal in the case of a linear model and an infinite ensemble size, it has been shown to work well in cases similar to ours (Annan et al., 2005a; Hargreaves et al., 2004).

The parameter estimation problem studied here is a steady state problem, somewhat different in detail (and in principle simpler) than the more conventional time-varying implementations of the EnKF. However, the prior assumption of substantial ignorance, combined with the nonlinearity of the model and high dimensionality of the parameter space being explored, means that a direct solution of the steady state problem does not work well. Therefore, an iterative scheme has been developed which repeats a cycle of ensemble inflation, data assimilation and model integration over a specified time interval, in order to converge to the final solution. (See the references mentioned above for the technical details.) As demonstrated in Annan et al. (2005a) and Annan and Hargreaves (2004), this iterative method converges robustly to the correct solution in identical twin testing. Further applications using real data have also been successful with a range of different models (e.g., Hargreaves et al., 2004; Annan et al., 2005b, c). The method is relatively efficient, requiring a total of approximately 100 times the equilibrium time of the model to converge, and it is exact in the case of a linear model

and a large ensemble size.

This method has already been used to calibrate the physical part of this model with long-term average climatological data to produce a reasonable representation of the preindustrial climate (Hargreaves et al., 2004). For this work we use the ensemble mean parameter set derived using the same method but with a slightly more recent version of the model (following the correction of an error in the equation of state for seawater, giving ~2 Sv stronger Atlantic meridional overturning compared to Hargreaves et al. (2004), and in closer agreement with observational estimates) to define the physical climate model. These physical parameters are kept fixed during the calibration of the biogeochemical model reported here.

As mentioned above, the EnKF ensemble randomly samples the probability distribution function defined by the model, data and prior assumptions. Therefore, the ensemble members do not themselves converge to the optimum but instead sample the region around it, with the ensemble mean being a good estimate of the optimum. Where all uncertainties are well defined, the spread of the ensemble members indicates the uncertainty surrounding this optimum. However, this is not the case here, since many model parameterizations are poorly understood and may be inadequate in various ways. A good example is the uncertainty surrounding the role of dust and the marine iron cycle (Jickells et al., 2005). The formulation of the biogeochemical model is thus inherently more uncertain than that of a physical model, and, at this stage, there is no clear way to estimate the true uncertainty of the calibrated model. We therefore use the EnKF to produce a single calibrated model version, taking the mean of this ensemble as an estimate of the best parameters.

The marine carbon cycle is calibrated against long-term average observations of $PO_4$ (Conkright et al., 2002) and ALK (Key et al., 2004) distributions in the ocean. We chose these data targets on the basis that $PO_4$ will help constrain the cycling of organic matter within the ocean, while ALK will (primarily) help constrain the cycling of $CaCO_3$ in the ocean. We assume that their observed distributions are relatively unaffected by anthropogenic change (Orr et al., 2005) (although see Feely et al., 2004). To create the

$PO_4$ and ALK assimilation "targets", we transformed the 3-D data-sets of Conkright et al. (2002) and Key et al. (2004]), respectively, to the GENIE-1 model grid, and salinity-normalized the data. For the surface data target, although the model surface layer is 175 m thick, the observed data is integrated only over the uppermost 75 m, which is assumed in the OCMIP-2 protocol to be the nominal "consumption" depth separating the production zone (above) from the consumption zone (below) for calculating surface boundary conditions (Najjar and Orr, 1999).

The calibration of the biogeochemistry used an ensemble size of 54, which was chosen primarily for computational convenience. Ocean chemistry was initialized with uniform concentrations of; 2244 $\mu$mol kg$^{-1}$ DIC (estimated pre-Industrial) (Key et al., 2000), 2363 $\mu$mol eq kg$^{-1}$ ALK (Key et al., 2000), 2.159 $\mu$mol kg$^{-1}$ $PO_4^{3-}$ (Conkright et al., 2001), and 169.6 $\mu$mol kg$^{-1}$ $O_2$ (Conkright et al., 2002). Initial concentrations of dissolved organic matter are zero, as are $\delta^{13}$C and $\delta^{14}$C. Atmospheric $pO_2$ was initially set at 0.2095 atm and allowed to evolve freely in response to net air-sea gas exchange thereafter. Atmospheric $CO_2$ was continually restored to a value of 278 ppm throughout the assimilation. The parameters we considered in the EnKF assimilation as well as our prior assumptions regarding their likely values are listed in Table 1.

### 3.2 Results of the EnKF assimilation

The mean and standard deviation of the ensemble values of the controlling biogeochemistry parameters are listed in Table 1. Most of the parameters showed only weak correlations in the posterior ensemble, with the striking exception of $r_0^{CaCO_3:POC}$ and $\eta$, as shown in Fig. 4. We can trace this relationship back to Eqs. (8) and (9), where it implies that $r_0^{CaCO_3:POC} \cdot (\Omega - 1)^{\eta}$ is close to being constant. We interpret this to mean that although total global production of carbonate is relatively tightly constrained by the data, the spatial variation, which is a function of local saturation state ($\Omega$) in the model, is not as well constrained.

We explored the sensitivity of the model calibration to the assimilated data by using

the ALK data of Goyet et al. (2000) as an alternative to Key et al. (2004). (We omitted assimilating surface model layer ALK in this case because the Goyet et al. (2000) data-set is valid only below the mixed layer depth in the ocean.) We found that the marine carbon cycle model and GLODAP $PO_4$ data set (Key et al., 2004) were less consistent with the Goyet et al. (2000) ALK distributions compared to the GLODAP ALK data (Key et al., 2004). Assimilation of the latter data rather than the former reduced the root mean square difference between model ALK and $PO_4$ fields taken together by about 10%. Most of the improvement occurred in the fit of the model to the ALK data set but there was also a slight improvement (1%) in the fit of the $PO_4$ data set to the model output. We interpret this in terms of the interpolation procedure used by Key et al. (2004) producing a more self-consistent data-set compared to the empirically based reconstruction of Goyet et al. (2000).

Analysis of ocean respiration patterns led Andersson et al. (2004) to propose a double exponential as a useful description for the profile of POC flux with depth. We tested a parameterization for the remineralization of POC in which each of the two fractions was assigned a characteristic (exponential decay) length scale. The mean EnKF calibrated remineralization length scales were 96 m and 994 m, compared to values of 55 m and ~2200 m determined by Andersson et al. (2004). However, the coarse vertical resolution of the model employed here means that we cannot place any confidence in length scales shorter than a few hundred meters. The improved fit to upper ocean $PO_4$ gradients using a double exponential in the EnKF comes at the expense of a rather negligible POC flux to the ocean floor because of the poor data constraint provided by the relatively weak gradients of $PO_4$ in the deep ocean (e.g., see Fig. 3). We thus retain the Eq. (6) parameterization (in which one of the fractions has a fixed and effectively infinite length scale) because achieving an appropriate POC flux to the ocean floor is critical to the determination of sedimentary carbonate content and organic carbon burial. (We address this further in the companion paper Ridgwell and Hargreaves, 2006[1].)

## 4 Discussion

### 4.1 The calibrated "baseline" state of the model

The calibrated model achieves appropriate zonally-averaged nutrient ($PO_4$) distributions for many regions of the ocean, particularly the Equatorial and North Atlantic, the Indian Ocean, and Equatorial Pacific and deep Pacific (Fig. 3). The predicted surface distribution of $PO_4$ (Figs. 5a, b) also agrees with the observations to a first-order (Conkright et al., 2002), with relatively high ($>0.5\,\mu mol\,kg^{-1}$) concentrations in the Southern Ocean, North Pacific, North Atlantic, and Eastern Equatorial Pacific, and nutrient depletion ($<0.5\,\mu mol\,kg^{-1}$) in the mid latitude gyres. However, over-estimated low latitude upwelling results in excess ($>0.5\,\mu mol\,kg^{-1}$) $PO_4$ in the Western Equatorial Pacific and Equatorial Indian Ocean. In addition, there is no representation of iron limitation, critical in the modern ocean in restricting nutrient depletion in the "High Nutrient Low Chlorophyll" (HNLC) regions of the ocean such as the North and Eastern Equatorial Pacific, and Southern Ocean (Jickells et al., 2005). The calibration must then strike a "compromise" – $PO_4$ uptake (scaled by the parameter, $u_0^{PO_4}$ in Eq. 3) must be sufficiently low that nutrients remain unused in the HNLC regions, yet at the same time, high enough to deplete nutrients elsewhere. The result is that $PO_4$ is generally slightly lower than observed in the HNLC regions but slightly too high elsewhere. Overall, global export production of particulate organic carbon (POC) is 8.91 GtC (PgC) $yr^{-1}$, consistent with recent estimates (e.g., Amount et al., 2003; Jin et al., 2006; Schmittner et al., 2005).

For alkalinity (ALK), we achieve a generally reasonable simile of the zonally-averaged distributions in each ocean basin (Fig. 3). The main areas of model-data mismatch concern surface concentrations. These are primarily caused by deficiencies in the climate model simulation of surface ocean salinities (see Hargreaves et al., 2004). This is because we assimilate salinity-normalized alkalinity, which means that deviations of model-predicted salinity from observations degrades the fidelity of sim-



BGD
3, 1313–1354, 2006



EGU

ulation of the (non salinity-normalized) ALK field. (The importance of salinity-related variations is much less for $PO_4$ because the biologically-induced range in concentrations is an order of magnitude greater.) Global pre-industrial $CaCO_3$ production is 1.21 PgC $yr^{-1}$, which falls towards the centre of the production budget uncertainty of 0.8–1.4 PgC $yr^{-1}$ proposed by Feely et al. (2004). It is also very close to the preferred estimate of 1.14 PgC $yr^{-1}$ diagnosed by Jin et al. (2006) from global nutrient and alkalinity distributions. The mean global $CaCO_3$:POC export ratio (Fig. 5c) is a little less than 0.14, supporting suggestions (Jin et al., 2006; Sarmiento et al., 2002; Yamanaka and Tajika, 1996) that the ratio is rather lower than the value of around 0.2–0.25 characterizing many models (e.g., Archer et al., 1998; Broecker and Peng, 1986; Heinze et al., 1999; Maier-Reimer, 1993). Of the predicted 1.21 PgC of biogenic carbonate exported annually from the surface ocean, approximately 0.62 PgC $yr^{-1}$ reaches 2000 m depth, slightly higher than estimates of 0.4 PgC $yr^{-1}$ based on sediment trap measurements (Feely et al., 2004).

With a mean ocean ALK of 2363 $\mu$mol eq $kg^{-1}$ (Key et al., 2004), a (pre-Industrial) atmospheric $CO_2$ concentration of 278 ppm requires a mean ocean DIC of 2214 $\mu$mol $kg^{-1}$ compared to an observationally-based estimate of 2244 $\mu$mol $kg^{-1}$ (Key et al., 2004). Some 14 $\mu$mol $kg^{-1}$ of this apparent DIC difference is explained by mean surface alkalinity being slightly lower than observed (2301 $\mu$mol eq $kg^{-1}$ compared to an average of 2310 $\mu$mol eq $kg^{-1}$ over the uppermost 75 m of the modern ocean (Conkright et al., 2002), itself mainly a consequence of the low surface salinities simulated by the climate model (particularly in the Atlantic) (Hargreaves et al., 2004). Use of a revised "Redfield ratio" value of 1:117 linking phosphorus and carbon in organic matter (Anderson and Sarmiento, 1994) increases DIC by ~7 $\mu$mol $kg^{-1}$, while using observed ocean surface temperatures (in place of climate model simulated temperatures) in the calculation of air-sea gas exchange accounts for another 2 $\mu$mol $kg^{-1}$ DIC. The residual model-data difference (9 $\mu$mol $kg^{-1}$ DIC) is comparable to the uncertainty in the GLODAP data-sets of ~5–10 $\mu$mol $kg^{-1}$ (Key et al., 2004). However, we cannot rule out convective ventilation or insufficient sea-ice extent in the South-

ern Ocean, lack of seasonality, and/or the thickness of the model surface ocean layer, contributing to driving the DIC inventory slightly too low.

### 4.2 The marine biogeochemical cycling of $O_2$

The model reproduces the main features of the observed distribution of dissolved oxygen ($O_2$) in the ocean (Fig. 6), with elevated concentrations associated with the sinking and subduction of cold and highly oxygenated waters in the North Atlantic, as well as the occurrence of intermediate depth minima at low latitudes in all three ocean basins. Deep ocean $O_2$ concentrations are almost everywhere correct to within $\sim 40\,\mu mol\,kg^{-1}$ of observations (Conkright et al., 2002). The area of greatest model-data mismatch concerns the ventilation of intermediate waters in the Southern Ocean and North Pacific. In addition, while the magnitude of $O_2$ depletion of the oxygen minimum zone in the northern Indian Ocean is correctly predicted, it lies at too shallow a depth and is too restricted in vertical extent. Overall, however, the quality of our $O_2$ simulation compares favorably with predictions made by considerably more computationally expensive ocean circulation models (e.g., Bopp et al., 2002; Meissner et al., 2005).

### 4.3 Ocean circulation and biogeochemical cycling in very coarse resolution models

While large-scale heat transports in the ocean are well captured (Hargreaves et al., 2004), the steady-state distribution of dissolved oxygen (Fig. 6) highlights the excess ventilation of intermediate depths above ca. 1500 m in parts of the Southern Ocean and North Pacific in the GENIE-1 model. We can demonstrate that ocean transport rather than processes associated with organic production and/or remineralization is primarily responsible by simulating the transient uptake of CFC-11 and CFC-12 from the atmosphere. We use a similar methodology to OCMIP-2 (Dutay et al., 2002), in which the partial pressure of CFCs in the atmosphere follow observations for the years 1932 to 1998 (Walker et al., 2000) and with air-sea gas exchange calculated explicitly according to Eqs. (12) and (13). The model-predicted 1994 global ocean CFC-11 inventory is



BGD
3, 1313–1354, 2006

$0.88\times10^9$ mol, compared to the observationally-based estimate of $0.55\pm0.08\times10^9$ mol (Willey et al., 2004; Key et al., 2004), with Southern Ocean intermediate depths accounting for more than half of the model-data mismatch.

Anthropogenic $CO_2$ uptake by the ocean can be similarly assessed by forcing atmospheric $CO_2$ to follow the historical trajectory between 1765 and 2000 (constructed from the data of Enting et al. (1990) up until 1994, and Keeling and Whorf (2004) thereafter), and allowing climate to respond. We find a year 1994 anthropogenic $CO_2$ inventory of 171 PgC compared to a recent data based estimate of 118±19 GtC (Sabine et al., 2004), with the main areas of model-data mismatch similar to CFC-11 and consistent with excess $O_2$ concentrations.

There may be fundamental limitations to how coarse a resolution a 3-D ocean circulation model may have and still simulate decadal-scale uptake processes accurately. This is because the stability of the water column at high latitudes appears to be very sensitive to the vertical resolution. For instance, it has recently been demonstrated (Müller et al., 2006) that a signification improvement in transient tracer uptake can be obtained by increasing the number of vertical levels from 8 to 32, although the use of observed climatological surface boundary conditions and separation of eddy-induced and isopycnal mixing effects may also have been critical in this. We have investigated this further by repeating the various OCMIP-2 transient tests with 16 rather than 8 levels in the ocean (Edwards and Marsh, 2005). For instance, radiocarbon properties of the deep ocean are relatively close to observations, with model-predicted $\Delta^{14}C$ below 2000 m in the Southern Ocean of ca. −140, and ca. −200 in the North Pacific.

Thus, simply increasing the vertical resolution appears to be an effective strategy in creating a more stable water column at high latitudes. However, this comes at a computational price because there is an approximate doubling of the number of cells in the ocean, while a thinner surface layer requires that air-sea gas exchange is updated more frequently to ensure numerical stability. Overall, these changes reduce the speed of a 16-level version of GENIE-1 Earth system model by a factor of about 3. To address century to millennial-scale (and longer) questions, particularly those involving interac-

tion with deep-sea sediments we retain the 8-level ocean by default, but recognize the limitations we have identified in 8-level vs. 16-levels, in representing some sub-decadal processes.

Finally, we confirm our assumptions regarding the century-scale (and beyond) applicability of an 8-level configuration by running an OCMIP-2 test, in which an abiotic ocean is brought to steady state with an atmospheric $CO_2$ concentration of 278 ppm, atmospheric $CO_2$ instantaneously doubled, and the invasion of $CO_2$ into the ocean then tracked for 1000 years (Orr, 2002). We find that atmospheric $CO_2$ concentrations diverge between our 8-level model and the OCMIP-2 models over the first few decades of uptake, but the trajectories re-converge thereafter (Fig. 7), making the century-scale (and longer) $CO_2$ behavior in GENIE-1 indistinguishable from the differing OCMIP-2 model behaviors. This is consistent with simulations we have made of radiocarbon distributions in the ocean (not shown) in which predicted (natural) $\Delta^{14}C$ properties of deep ocean water masses also fall within the range of OCMIP-2 model behavior (Matsumoto et al., 2004). That we reproduce the year 2100 prediction for the strength of "$CO_2$-calcification" feedback (the enhancement of $CO_2$ uptake from the atmosphere due to reduced calcification) made by a much higher resolution ocean model (Ridgwell et al., 2006[2]) also supports our assertion regarding the sphere of applicability of the fast 8-level version of the GENIE-1 model.

## 5 Conclusions

We have constructed a 3-D ocean based Earth System Model that includes key feedbacks between marine carbon cycling, atmospheric $CO_2$, and climate, yet even when simulating 12 biogeochemical tracers in the ocean together with the exchange with the atmosphere of 6 gaseous tracers, achieves better than 1000 yr simulated per (2.4 GHz) CPU hour on a desktop computer. The computational speed of the GENIE-1 model has enabled us to calibrate via an Ensemble Kalman Filter (EnKF) method the critical parameters controlling marine carbon cycling. The EnKF has also allowed us to judge the

consistency of available global alkalinity data-sets with our mechanistic representation of global biogeochemical cycling, and has determined the a priori unknown relationship between $\eta$ and $r_0^{CaCO_3:POC}$ in our parameterization of carbonate production. Because our results highlight the importance of global biogeochemical cycling in providing a sensitive diagnostic of ocean circulation in models, we propose that more physically realistic models might be achieved by "co-tuning" key physical and biogeochemical parameters.

Global particulate organic carbon and inorganic (carbonate) carbon export predicted by the calibrated model is consistent with recent data- and model-based estimates. Furthermore, despite the very coarse resolution of the ocean model, the distribution of dissolved $O_2$ in the ocean generally compares favorably with the data and with the results of much more computationally expensive 3-D ocean circulation models. Overall, the speed and multi-tracer capabilities make the GENIE-1 model a viable alternative to marine biogeochemical box models for questions regarding the controls on atmospheric $CO_2$ over all but the very longest (>100 000 years) time-scales.

*Acknowledgements.* A. Ridgwell acknowledges support from Canada Research Chairs and Canadian Foundation for Climate and Atmospheric Sciences. Development of the model was supported by the NERC e-Science programme (NER/T/S/2002/00217) through the Grid ENabled Integrated Earth system modelling (GENIE) project (http://www.genie.ac.uk) and by the Tyndall Centre for Climate Change Research (Project TC IT 1.31). Computer facilities for the EnKF calculations were provided by JAMSTEC. We are indebted to the generosity of OCMIP-2 participants who made their unpublished model $CO_2$ results available to us; A. Ishida and Y. Yamanaka at the Frontier Research Center for Global Change, Japan (formally "IGCR"), Fortunat Joos at Climate and Environmental Physics, Bern, and R. Schlitzer of AWI- Bremerhaven.

## References

Anderson, L. and Sarmiento, J.: Redfield ratios of remineralization determined by nutrient data analysis, Global Biogeochem. Cycles, 8, 65–80, doi:10.1029/93GB03318, 1994.

Andersson, J. H., Wijsman, J. W. M., Herman, P. M. J., et al.: Respiration patterns in the deep ocean, Geophys. Res. Lett., 31, L03304, doi:10.1029/2003GL018756, 2004.
Annan, J. D. and Hargreaves, J. C.: Efficient parameter estimation for a highly chaotic system, Tellus A, 56, 520–526, 2004.
Annan, J. D., Hargreaves, J. C., Edwards, N. R., and Marsh, R.: Parameter estimation in an intermediate complexity Earth System Model using an ensemble Kalman filter, Ocean Modell., 8, 135–154, 2005a.
Annan, J. D., Lunt, D. J., Hargreaves J. C., and Valdes, P. J.: Parameter Nonlinear Processes in Geophysics, 12, 363–371, 2005b.
Annan, J. D., Hargreaves, J. C., Ohgaito, R., Abe-Ouchi, A., and Emori, S.: Efficiently constraining climate sensitivity with ensembles of paleoclimate simulations, SOLA, 1, 181–184, 2005c.
Archer, D.: Modeling the calcite lysocline, J. Geophys. Res., 96, 17 037–17 050, 1991.
Archer, D., Kheshgi, H., and Maier-Reimer, E.: Dynamics of fossil fuel $CO_2$ neutralization by marine $CaCO_3$, Global Biogeochem. Cycles, 12, 259, 1998.
Archer, D., Winguth, A., Lea, D., and Mahowald, N.: What caused the glacial/interglacial atmospheric $pCO_2$ cycles?, Rev. Geophys., 38, 159–189, 2000.
Archer, D. E., Martin, P. A., Milovich, J., Brovkin, V., Plattner, G.-K., and Ashendel, C.: Model sensitivity in the effect of Antarctic sea ice and stratification on atmospheric $pCO_2$, Paleoceanography, 18, 1012, doi:10.1029/2002PA000760, 2003.
Archer, D., Martin, P., Buffet, B., et al.: The importance of ocean temperature to global biogeochemistry, Eeart Plant. Sci. Lett., 222, 333–348, 2004.
Archer, D.: Fate of fossil fuel $CO_2$ in geologic time, J. Geophys. Res., 110, C09S05, doi:10.1029/2004JC002625, 2005.
Aumont, O., Maier-Reimer, E., Blain, S., and Monfray, P.: An ecosystem model of the global ocean including Fe, Si, P colimitations, Global Biogeochem. Cycles, 17, 1060, doi:10.1029/2001GB001745, 2003.
Barker, S., Higgins, J. A., and Elderfield, H.: The future of the carbon cycle: review, calcification response, ballast and feedback on atmospheric $CO_2$, Philosophical Trans. Royal Soc. A, 361, 1977–1999, 2003.
Bijma, J., Spero, H. J., and Lea, D.W.: Reassessing foraminiferal stable isotope geochemistry: Impact of the oceanic carbonate system (Experimental Results), in: Use of proxies in paleoceanography: Examples from the South Atlantic, edited by: Fischer, G., Wefer, G.,

Springer-Verlag Berlin Heidelberg, 489–512, 1999.
Bopp, L., LeQuéré, C., Heimann, M., Manning, A. C., and Monfray, P.: Climate-induced oceanic oxygen fluxes: Implications for the contemporary carbon budget, Global Biogeochem. Cycles, 16, 1022, doi:10.10292001GB, 2002.
Bopp, L., Kohfeld, K. E., Le Quere, C., and Aumont, O.: Dust impact on marine biota and atmospheric $CO_2$ during glacial periods, Paleoceanography, 18, 1046, doi:10.1029/2002PA000810, 2003.
Broecker, W. S. and Peng, T-H.: Glacial to interglacial changes in the operation of the global carbon cycle, Radiocarbon, 28, 309–327, 1986.
Burton, E. A. and Walter, L. M.: Relative precipitation rates of aragonite and mg calcite from seawater – Temperature or carbonate ion control, Geology 15, 111–114, 1987.
Caldeira, K. and Wickett, M. E.: Anthropogenic carbon and ocean *p*H, Nature 425, 365, 2003.
Cameron, D. R., Lenton, T. M., Ridgwell, A. J., Shepherd, J. G., Marsh, R. J., and the GENIE team: A factorial analysis of the marine carbon cycle controls on atmospheric $CO_2$, Global Biogeochem. Cycles, 19, GB4027, doi:10.1029/2005GB002489, 2005.
Claussen, M., Mysak, L. A., Weaver, A. J., et al.: Earth system models of intermediate complexity: closing the gap in the spectrum of climate system models, Climate Dyamics., 18, 579–586, 2002.
Conkright M. E., Antonov, J. I., Baranov, O. K., et al.: World Ocean Database 2001, Volume 1: Introduction. edited by: Levitus, S., NOAA Atlas, NESDIS 42, U.S. Government Printing Office, Washington, D.C., 167 pp, 2002.
Cox, P. M., Betts, R. A., Jones, C. D., et al.: Acceleration of global warming due to carbon-cycle feedbacks in a coupled climate model, Nature, 408, 184–187, 2000.
Delille, B., Harlay, J., Zondervan, I., et al.: Response of primary production and calcification to changes of $pCO_2$ during experimental blooms of the coccolithophorid *Emiliania huxleyi*, Global Biogeochem. Cycles, 19, GB2023, doi:10.1029/2004GB002318, 2005.
Dickson, A. G.: An exact definition of total alkalinity and a procedure for the estimation of alkalinity and total inorganic carbon from titration data, Deep-Sea Res., 28, 609–623, 1981.
Dickson, A. G. and Millero, F. J.: A comparison of the equilibrium constants for the dissociation of carbonic acid in seawater media, Deep-Sea Res., 34, 1733–1743, 1987.
Doney, S. C., Lindsay, K., Caldeira, K., et al.: Evaluating global ocean carbon models: The importance of realistic physics, Global Biogeochem. Cycles, 18, GB3017, doi:10.1029/2003GB002150, 2004.

Dutay, J.-C., Bullister, J. L., Doney, S. C., et al.: Evaluation of ocean model ventilation with CFC-11: comparison of 13 global ocean models, Ocean Modell., 4, 89–120, 2002.
Edwards, N. R. and Marsh, R.: Uncertainties due to transport-parameter sensitivity in an efficient 3-D ocean-climate model, Climate Dynamics, 24, 415–433, 2005.
Enting, I. G., Wigley, T. M. L., and Heimann, M.: "Future Emissions and Concentrations of Carbon Dioxide: Key Ocean/Atmosphere/Land Analyses", CSIRO Division of Atmospheric Research Technical Paper No. 31, Commonwealth Scientific and Industrial Research Organisation, Aspendale, Australia, 1994.
Evensen, G.: Sequential data assimilation with a nonlinear quasigeostrophic model using Monte Carlo methods to forecast error statistics, J. Geophys. Res., 99, 10 143–10 162, 1994.
Feely, R. A., Sabine, C. L., Lee, K., et al.: Impact of anthropogenic $CO_2$ on the $CaCO_3$ system in the oceans, Science, 305, 362–366, 2004.
Gildor, H., Tziperman, E., and Toggweiler, J. R.: Sea ice switch mechanism and glacial-interglacial $CO_2$ variations, Global Biogeochem. Cycles, 16, 1032, doi:10.1029/2001GB001446, 2002.
Gordon, C., Cooper, C., Senior, C. A., et al.: The simulation of SST, sea ice extents and ocean heat transport in a version of the Hadley Centre coupled model without flux adjustments, Climate Dynamics, 16, 147–168, 2000.
Goyet, C., Healy, R., and Ryan, J.: Global Distribution of Total Inorganic Carbon and Total Alkalinity Below the Deepest Winter Mixed Layer Depths. Carbon Dioxide Information Analysis Center, May 2000.
Hargreaves, J. C., Annan, J. D., Edwards, N. R., and Marsh, R.: Climate forecasting using an intermediate complexity Earth System Model and theEnsemble Kalman Filter, Climate Dynamics, 23, 745–760, 2004.
Heinze, C., Maier-Reimer, E., Winguth, A. M. E., and Archer, D.: A global oceanic sediment model for long-term climate studies, Global Biogeochem. Cycles, 13, 221–250, 1999.
Heinze, C.: Simulating oceanic $CaCO_3$ export production in the greenhouse, Geophys. Res. Lett., 31, L16308, doi:10.1029/2004GL020613, 2004.
Hesshaimer, V., Heimann, M., and Levin, I.: Radiocarbon evidence for a smaller oceanic carbon dioxide sink than previously believed, Nature, 370, 201–203, 1994.
Hotinski, R., Bice, K., Kump, L., Najjar, R., and Arthur, M.: Ocean stagnation and end-Permian anoxia, Geology, 29, 7–10, 2001.

Jickells, T. D., An, Z. S., Andersen, K. K., et al.: Global Iron Connections Between Desert Dust, Ocean Biogeochemistry, and Climate, Science, 308, 67–71, 2005.
Jin, X., Gruber, N., Dunne, J., Sarmiento, J. L., and Armstrong, R. A.: Diagnosing the contribution of phytoplankton functional groups to the production and export of POC, $CaCO_3$ and opal from global nutrient and alkalinity distributions, Global Biogeochem. Cycles, 20, GB2015, doi:10.1029/2005GB002532, 2006.
Joos, F., Orr, J. C., and Siegenthaler, U.: Ocean carbon transport in a box-diffusion versus a general circulation model, J. Geophys. Res., 102, 12 367–12 388, 1997.
Keeling, C.D. and Whorf, T. P.: Atmospheric $CO_2$ records from sites in the SIO air sampling network. In Trends: A Compendium of Data on Global Change. Carbon Dioxide Information Analysis Center, Oak Ridge National Laboratory, U.S. Department of Energy, Oak Ridge, Tenn., USA, http://cdiac.esd.ornl.gov/trends/co2/sio-mlo.htm, 2004.
Key, R. M., Kozyr, A., Sabine, C. L., et al.: A global ocean carbon climatology: Results from Global Data Analysis Project (GLODAP), Global Biogeochem. Cycles, 18, GB4031, doi:10.1029/2004GB002247, 2004.
Khalil, M. A. K. and Rasmussen, R. A.: Ocean-air exchange of atmospheric trace gases, Rep. 01-1097, Dep. of Phys., Portland State Univ., Portland, Oreg., 1998.
Kleypas, J. A., Buddemeier, R. W., Archer, D., et al.: Geochemical consequences of increased atmospheric carbon dioxide on coral reefs, Science, 284, 118, 1999.
Langdon, C. and Atkinson, M. J.: Effect of elevated $pCO_2$ on photosynthesis and calcification of corals and interactions with seasonal change in temperature/irradiance and nutrient enrichment, J. Geophys. Res., 110, C09S07, doi:10.1029/2004JC002576, 2005.
Lenton, T. M., Williamson, M. S., Edwards, N. R., Marsh, R. J., Price, A. R., Ridgwell, A. J., Shepherd, J. G., Cox, S. J., and the GENIE team: Millennial timescale carbon cycle and climate change in an efficient Earth system model, Climate Dynamics, 687–711, doi:10.1007/s00382-006-0109-9, 2006.
Lewis, E. and Wallace, D. W. R.: Program Developed for $CO_2$ System Calculations. ORNL/CDIAC-105. Carbon Dioxide Information Analysis Center, Oak Ridge National Laboratory, U.S. Department of Energy, Oak Ridge, Tennessee, 1998.
Maier-Reimer, E.: Geochemical cycles in an ocean general circulation model. Pre-industrial tracer distributions, Global Biogeochem. Cycles, 7, 645–677, 1993.
Marchal, O., Stocker, T. F., and Joos, F.: A latitude-depth, circulation biogeochemical ocean model for paleoclimate studies. Development and sensitivities, Tellus Series B – Physical

and Physical Meteorology, 50B, 290–316, 1998.
Matsumoto, K., Sarmiento, J. L., Key, R. M., et al.: Evaluation of ocean carbon cycle models with data-based metrics, Geophys. Res. Lett., 31, l07303, doi:10.1029/2003GL018970, 2004.
Meissner, K., Galbraith, E. D., and Voelker, C.: Denitrification under glacial and interglacial conditions: a physical approach, Paleoceanography, 20, PA3001, doi:10.1029/2004PA001083, 2005.
Mehrbach, C., Culberson, C. H., Hawley, J. E., and Pytkowicz, R. M.: Measurement of the apparent dissociation constants of carbonic acid in seawater at atmospheric pressure, Limnology and Oceanography, 18, 897–907, 1873.
Millero, F. J.: The thermodynamics of seawater. Part I. The PVT properties, Ocean Sci. Eng., 7, 403–460, 1982.
Millero, F. J.: The thermodynamics and kinetics of the hydrogen sulfide system in natural waters, Mar. Chem., 18, 121–147, 1986.
Millero, F. J.: Thermodynamics of the carbon dioxide system in the oceans, Geochemica et Cosomochimica Acta, 59, 661–677, 1995.
Mook, W. G.: $^{13}C$ in atmospheric $CO_2$, Netherlands J. Sea Res., 20, 211–223, 1986.
Moore, J. K., Doney, S. C., Kleypas, J. A., et al.: An intermediate complexity marine ecosystem model for the global domain, Deep-Sea Res. II, 49, 403–462, 2002.
Müller, S. A., Joos, F., Edwards, N. R., and Stocker, T. F.: Water mass distribution and ventilation time scales in a cost-efficient, 3-dimensional ocean model, J. Climate, in press, 2006.
Najjar, R. G., Sarmiento, J. L., and Toggweiller, J. R.: Downward transport and fate of organic matter in the ocean: Simulations with a General Circulation Model, Global Biogeochem. Cycles, 6, 45–76, 1992.
Najjar, R. G. and Orr, J. C.: Biotic-HOWTO. Internal OCMIP Report, LSCE/CEA Saclay, Gif-sur-Yvette, France, 15 pp., 1999.
Opdyke, B. N. and Wilkinson, B. H.: Carbonate mineral saturation state and cratonic limestone accumulation, Am. J. Science, 293, 217–234, 1993.
Orr, J. C.: Global Ocean Storage of Anthropogenic Carbon, 116 pp., Inst. Pierre Simon Laplace, Gif-sur-Yvette, France, 2002.
Orr, J. C., Fabry, V. J., Aumont, O., et al.: Anthropogenicocean acidification over the twenty-first century and its impact on calcifying organisms, Nature, 437, 681–686, 2005.
Parekh, P., Follows, M. J., and Boyle, E. A.: Modeling the global ocean iron cycle, Global

Biogeochem. Cycles, 18, GB1002, doi:10.1029/2003GB002061, 2004.
Parekh, P., Follows, M. J., and Boyle, E. A.: Decoupling of iron and phosphate in the global ocean, Global Biogeochem. Cycles, 19, GB2020, doi:10.1029/2004GB002280, 2005.
Plattner, G. K., Joos, F., Stocker, T. F., and Marchal, O.: Feedback mechanisms and sensitivities of ocean carbon uptake under global warming, Tellus B, 53, 564–592, 2001.
Rau, G. H., Riebesell, U., and Wolf-Gladrow, D.: A model of photosynthetic $^{13}C$ fractionation by marine phytoplankton based on diffusive molecular $CO_2$ uptake, Mar. Ecol. Progress Ser., 133, 275–285, 1996.
Rau, G. H., Riebesell, U., and Wolf-Gladrow, D.: $CO_{2aq}$-dependent photosynthetic $^{13}C$ fractionation in the ocean: A model versus measurements, Global Biogeochem. Cycles, 11, 267–278, 1997.
Redfield, A. C., Ketchum, B. H., and Richards, F. A.: The influence of organisms in the composition of sea water, in: The Sea, Hill, N. M., 26–77, Wiley-Interscience, New York, 1963.
Ridgwell, A. J.: Glacial-interglacial perturbations in the global carbon cycle, PhD thesis, Univ. of East Anglia at Norwich, UK, (http://www.seao2.org/pubs/ridgwell_2001.pdf), 2001.
Ridgwell, A.: Changes in the mode of carbonate deposition: Implications for Phanerozoic ocean chemistry, Mar. Geol., 217, 339, 2005.
Ridgwell, A. and Zeebe, R. E.: The role of the global carbonate cycle in the regulation and evolution of the Earth system, Earth Planet. Sci. Lett., 234(3–4), 299–315, 2005.
Riebesell, U., Zondervan, I., Rost, B., Tortell, P. D., Zeebe, R. E., and Morel, F. M. M.: Reduced calcification of marine plankton in response to increased atmospheric $CO_2$, Nature, 407, 364–367, 2000.
Sabine, C. L., Feely, R. A., Gruber, N., et al.: The Oceanic Sink for Anthropogenic $CO_2$, Science, 305, 367–371, 2004.
Sarmiento, J. L. and Toggweiler, J. R.: A new model for the role of the oceans in determining atmospheric $pCO_2$, Nature, 308, 621–624, 1984.
Sarmiento, J. L., Hughes, T. M. C., Stouffer, R. J., and Manabe, S.: Simulated response of the ocean carbon cycle to anthropogenic climate warming, Nature, 393, 245–249, 1998.
Sarmiento, J. L., Dunne, J., Gnanadesikan, A., et al.: A new estimate of the $CaCO_3$ to organic carbon export ratio, Global Biogeochem. Cycles, 16, 1107, doi:10.1029/2002GB001919, 2002.
Schmittner, A.: Decline of the marine ecosystem caused by a reduction in the Atlantic overturning circulation, Nature, 434, 628–633, 2005.

Schmittner, A., Oschlies, A., Giraud, X., Eby, M., and Simmons, H. L.: A global model of the marine ecosystem for long-term simulations: Sensitivity to ocean mixing, buoyancy forcing, particle sinking, and dissolved organic matter cycling, Global Biogeochem. Cycles, 19, GB3004, doi:10.1029/2004GB002283, 2005.

Schiebel, R.: Planktic foraminiferal sedimentation and the marine calcite budget, Global Biogeochem. Cycles, 16, 1065, doi:10.1029/2001GB001459, 2002.

Schlitzer, R.: Carbon export fluxes in the Southern Ocean: Results from inverse modeling and comparison with satellite-based estimates, Deep Sea Res., 49, 1623–1644, 2002.

Shaffer G., Bendtsen, J., and Ulloa, O.: Fractionation during remineralization of organic matter in the ocean, Deep Sea Res., 46, 185–204, 1999.

Siegenthaler, U., Stocker, U. T. F., Monnin, E., et al.: S table Carbon Cycle–Climate Relationship During the Late Pleistocene, Science, 310, 1313–1317, 2005.

Smith, H. J., Fischer, H., Wahlen, M., Mastroianni, D., and Deck, B.: Dual modes of the carbon cycle since the Last Glacial Maximum, Nature, 400, 248–250, 1999.

Stocker, T. F., Wright, D. G., and Mysak, L. A.: A zonally averaged, coupled ocean-atmosphere model for paleoclimate studies, J. Clim., 5, 773–797, 1992.

Stuiver, M. and Polach, H. A.: Reporting of $^{14}C$ Data, Radiocarbon, 19, 355–363, 1977.

Trenberth, K., Olson, J., and Large, W.: A Global Ocean Wind Stress Climatology based on ECMWF Analyses. Tech. Rep. NCAR/TN-338+STR, National Center for Atmospheric Research, Boulder, Colorado, 1989.

Walker, S. J., Weiss, R. F., and Salameh, P. K.: Reconstructed histories of the annual mean atmospheric mole fractions for halocarbons CFC-11,CFC-12,CFC-113,and carbon tetrachloride, J. Geophys. Res., 105, 14 285–14 296, 2000.

Wanninkhof, R.: Relationship between wind-speed and gas-exchange over the ocean, J. Geophys. Res., 97, 7373–7382, 1992.

Weaver, A. J., Eby, M., Wiebe, E. C., et al.; The UVic Earth System Climate Model: Model Description, Climatology, and Applications to Past, Present and Future Climates, Atmos.-Ocean, 39, 361–428, 2001.

Willey, D. A., Fine, R. A., Sonnerup, R. E., et al.: Global oceanic chlorofluorocarbon inventory, Geophys. Res. Lett., 31, L01303, doi:10.1029/2003GL018816, 2004.

Yamanaka, Y. and Tajika, E.: The role of the vertical fluxes of particulate organic matter and calcite in the oceanic carbon cycle: Studies using an ocean biogeochemical general circulation model, Global Biogeochem. Cycles, 10, 361–382, 1996.

Yool, A. and Tyrrell, T.: Implications for the history of Cenozoic opal deposition from a quantitative model, Palaeogeography Palaeoclimatology Palaeoecology, 218, 239–255, doi:10.1016/j.palaeo.2004.12.017, 2005.

Zachos, J. C., Röhl, J. C., Schellenberg, S. A., et al.: Rapid Acidification of the Ocean During the Paleocene-Eocene Thermal Maximum, Science, 308, 1611–1615, 2005.

Zeebe, R. E. and Wolf-Gladrow, D.: $CO_2$ in seawater: Equilibrium, kinetics, isotopes, Elsevier Oceanographic Series 65, Elsevier, New York, 2001.

Zeebe, R. E. and Westbroek, P.: A simple model for the $CaCO_3$ saturation state of the ocean: The "Strangelove," the "Neritan," and the "Cretan" Ocean, Geochem. Geophys. Geosyst., 4, 1104, doi:10.1029/2003GC000538, 2003.

Zhang, J.-Z. and Millero, F. J.: The products from the oxidation of $H_2S$ in seawater, Geochimica et Cosmochimica Acta, 57, 1705–1718, 1993.

Zhang, J., Quay, P. D., and Wilbur, D. O.: Carbon isotope fractionation during gas-water exchange and dissolution of $CO_2$, Geochimica et Cosmochimica Acta, 59, 107–115, 1995.

Zhang R., Follows, M. J., Grotzinger, J., and Marshall, J. C.: Could the Late Permian, deep ocean have been Anoxic?, Paleoceanography, 16, 317–329, 2001.

Zhang, R., Follows, M. J., and Marshall, J.: Reply to Comment by Roberta M. Hotinski, Lee R. Kump, and Karen L. Bice on "Could the Late Permian deep ocean have been anoxic?", Paleoceanography, 18, 1095, doi:10.1029/2002PA000851, 2003.

Zondervan, I., Zeebe, R. E., Rost, B., and Riebesell, U.: Decreasing marine biogenic calcification: A negative feedback on rising atmospheric $pCO_2$, Global Biogeochem. Cycles, 15, 507–516, 2001.

**Table 1.** EnKF calibrated biogeochemical parameters in the GENIE-1 model.

| Name | Prior assumptions (mean and range[a]) | Final value[b] | Description |
|---|---|---|---|
| $u_0^{PO_4}$ | 1.65 $\mu$mol kg$^{-1}$ yr$^{-1}$ (0.3–3.0) | 1.91 $\mu$mol kg$^{-1}$ yr$^{-1}$ | maximum $PO_4$ uptake (removal) rate (Eq. 3) |
| $K^{PO_4}$ | 0.2 $\mu$mol kg$^{-1}$ (0.1–0.3) | 0.21 $\mu$mol kg$^{-1}$ | $PO_4$ Michaelis-Menton half-saturation concentration (Eq. 3) |
| $r^{POC}$ | 0.05 (0.02–0.08) | 0.055 | initial proportion of POC export as fraction #2 (Eq. 6) |
| $l^{POC}$ | 600 m (200–1000) | 556 m | $e$-folding remineralization depth of POC fraction #1 (Eq. 6) |
| $r_0^{CaCO_3:POC}$ | 0.036 (0.015–0.088)[c] | 0.022 | $CaCO_3$:POC: export rain ratio scalar (Eq. 8) |
| $\eta$ | 1.5 (1.0–2.0) | 1.28 | thermodynamic calcification rate power (Eq. 9) |
| $r^{CaCO_3}$ | 0.4 (0.2–0.6) | 0.489 | initial proportion of $CaCO_3$ export as fraction #2 (Eq. 11) |
| $l^{CaCO_3}$ | 600 m (200–1000) | 1055 | $e$-folding remineralization depth of $CaCO_3$ fraction #1 (Eq. 11) |

[a]The range is quoted as 1 standard deviation either side of the mean,
[b]quoted as the mean of the entire EnKF ensemble,
[c]assimilation was carried out on a $\log_{10}$ scale.



BGD
3, 1313–1354, 2006



EGU

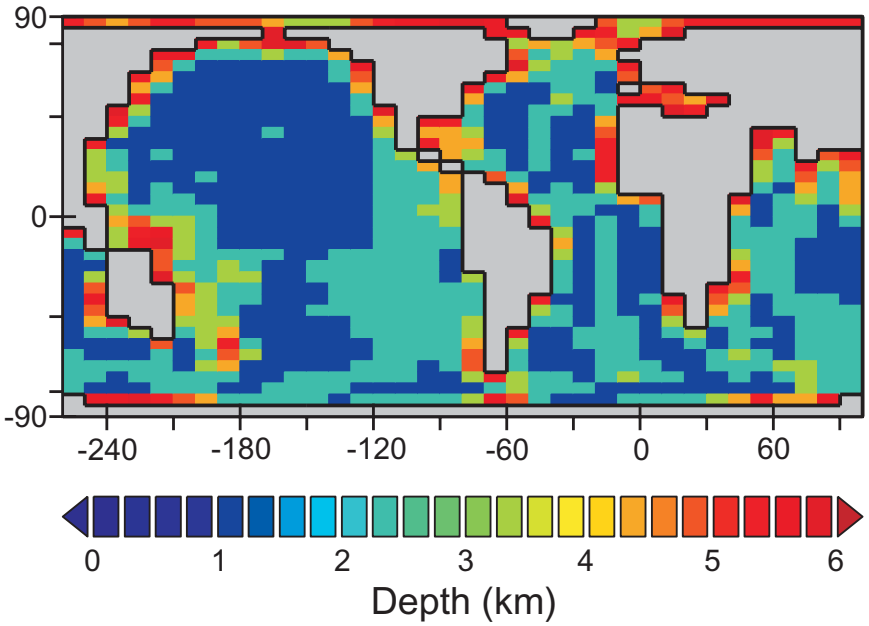


**Fig. 1.** Gridded continental configuration and ocean bathymetry of the 8-level, 36×36 equal-area grid version of the GENIE-1 model.



BGD
3, 1313–1354, 2006

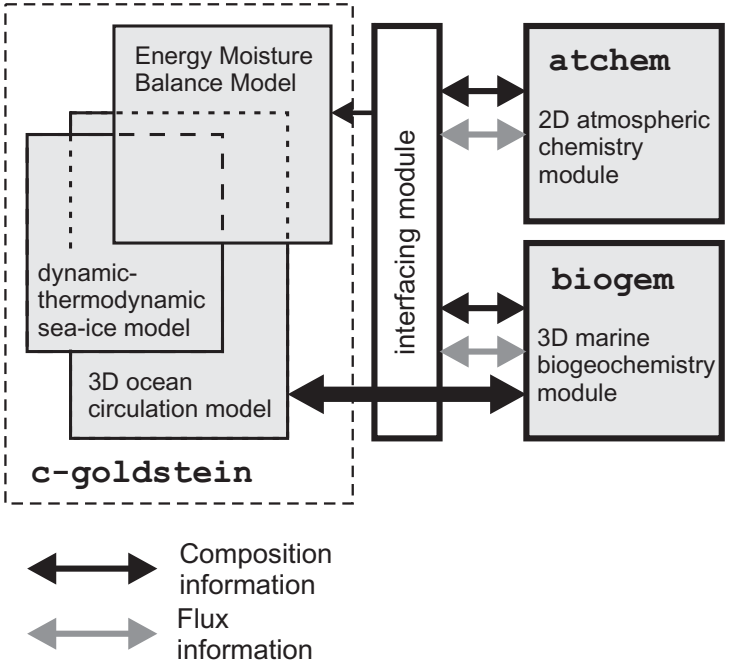


**Fig. 2.** Schematic of the relationship between the different model components comprising GENIE-1. Arrows represent the coupling of compositional information (black) and fluxes (grey). The bold highlights indicate the biogeochemical extensions described in this paper to the climate model (C-GOLDSTEIN) (Edwards and Marsh, 2005). The current implementation of the module ATCHEM (not described in the text) is rather trivial. (It consists of a 2-D 36×36 atmospheric grid storing atmospheric composition, together with a routine to homogenize composition across the grid each time-step.) The efficient numerical terrestrial scheme ENTS and modifications to the EMBM described in Williamson et al. (2006) are not used in this study, so that the land surface is essentially passive.



BGD
3, 1313–1354, 2006



EGU

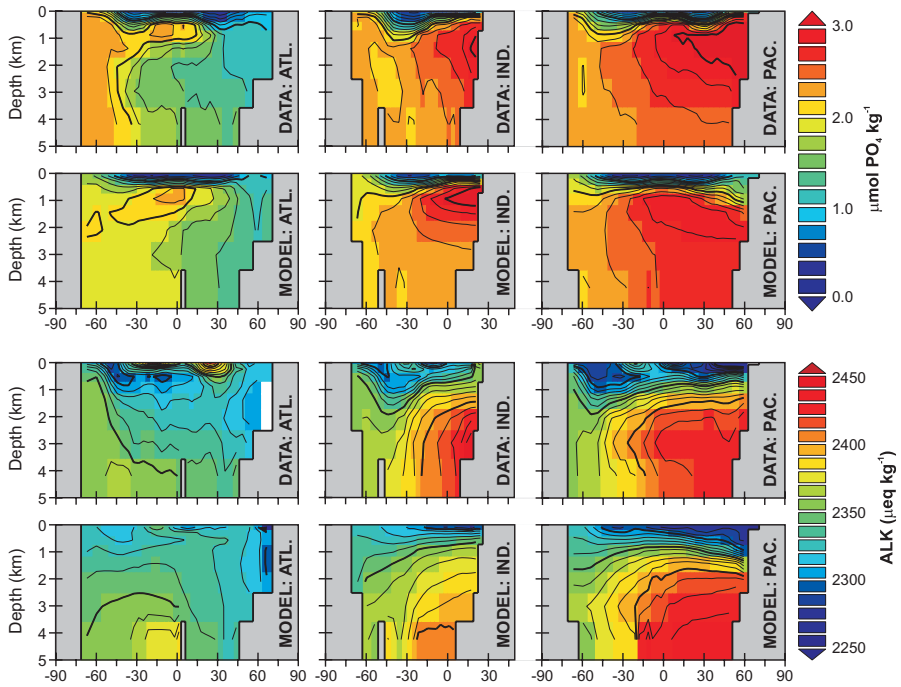


**Fig. 3.** Data assimilation of $PO_4$ and ALK. The top panel shows the basin averaged meridional-depth distribution of phosphate ($PO_4$), with the model simulation immediately below the respective observations (Conkright et al., 2002). The bottom panel shows the basin averaged meridional-depth distributions of alkalinty (ALK) (Key et al., 2004). Note that we plot this data as actual concentrations, whereas the assimilation is carried out on salinity-normalized values.



BGD
3, 1313–1354, 2006



EGU

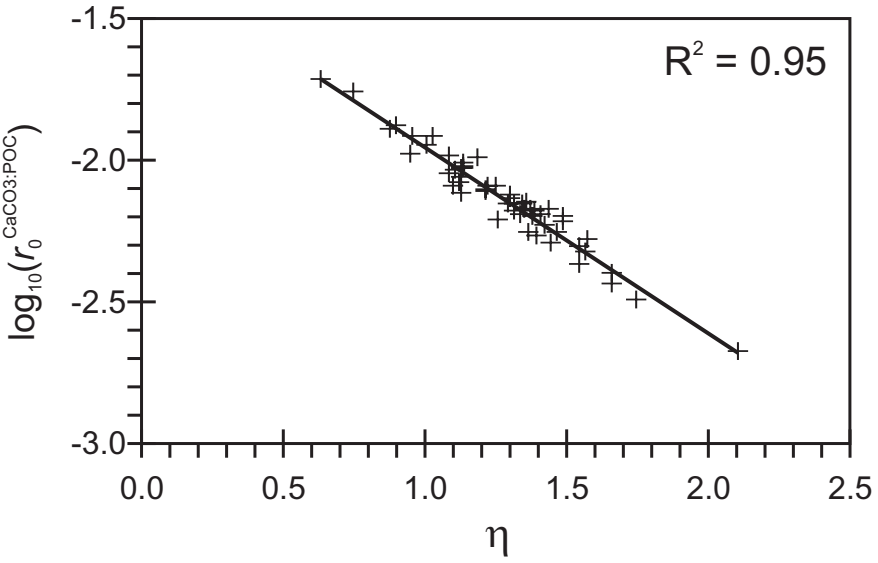


**Fig. 4.** Relationship between the parameters controlling $CaCO_3$ production. The values of $r_0^{CaCO_3:POC}$ and $\eta$ (Eq. 8) are plotted for all 54 ensemble members (crosses), as well as the best-fit relationship between them (solid line); $\log_{10}\left(r_0^{CaCO_3:POC}\right) = -0.6564 \cdot \eta - 1.2963$.



BGD
3, 1313–1354, 2006

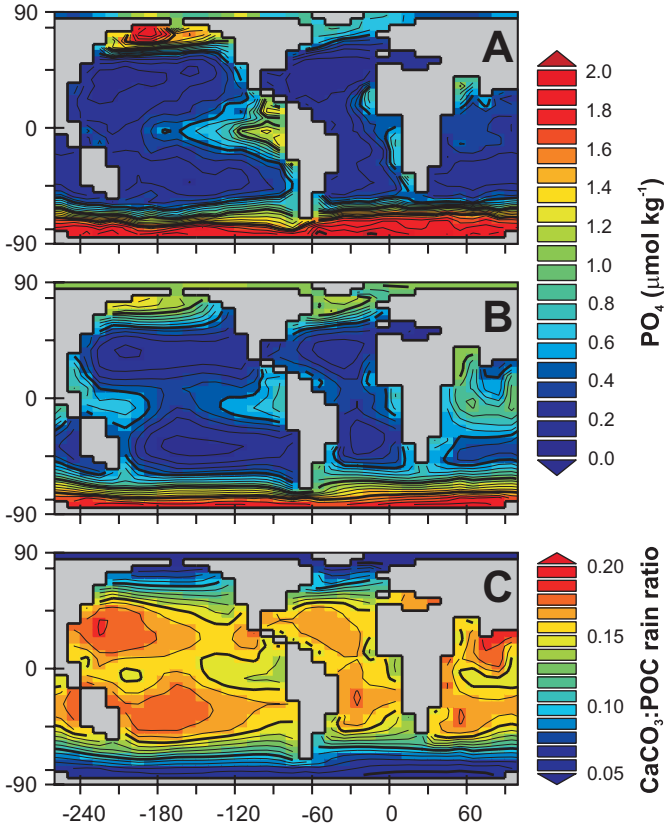


**Fig. 5.** Surface ocean properties. **(a)** Observed $PO_4$ concentrations in the surface ocean (integrated over the uppermost 75 m) (Conkright et al., 2002) compared to the model surface layer predictions **(b)**. **(c)** The predicted distribution of $CaCO_3$:POC export ratio.



BGD
3, 1313–1354, 2006

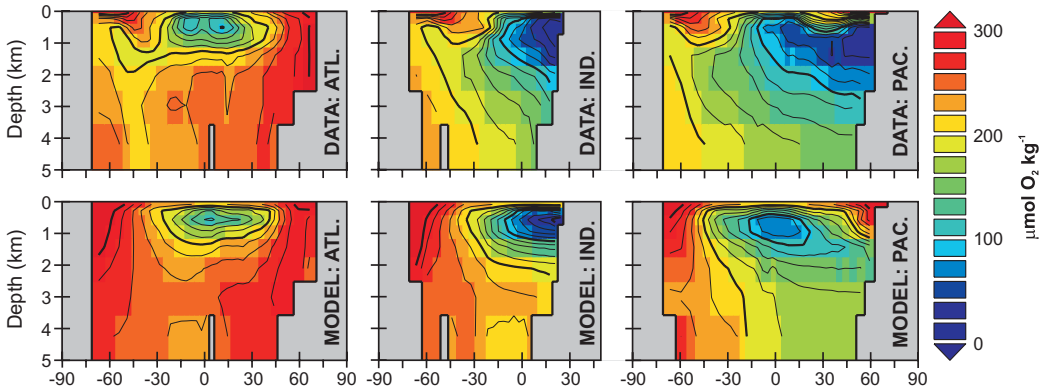


**Fig. 6.** Basin averaged meridional-depth distributions of dissolved oxygen in the ocean; observed (top) (Conkright et al., 2002) and model-simulated for the year 1994 (bottom).



BGD

3, 1313–1354, 2006

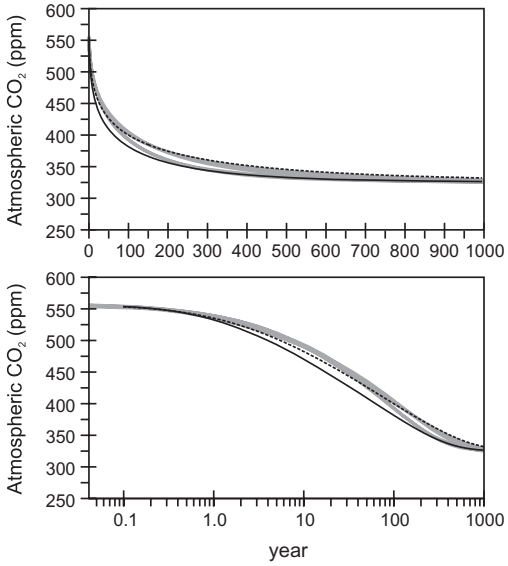


**Fig. 7.** Ocean $CO_2$ invasion behavior. Predicted evolution of atmospheric $CO_2$ following an instantaneous doubling to 556 ppm. The atmospheric $CO_2$ behavior of GENIE-1 is consistent with the four ocean carbon cycle models which ran this experiment out as part of OCMIP-2 (Doney et al., 2004). The OCMIP-2 models are those of; Schlitzer (2002); Yamanaka and Tajika (1996); Gordon et al. (2000); and Stocker et al. (1992). We deliberately do not differentiate between the different OCMIP-2 models here to highlight the comparison between GENIE-1 and models having much greater horizontal and/or vertical resolution, rather than discuss the reasons for the differences amongst the OCMIP-2 models. All OCMIP-2 trajectories are therefore plotted as identical grey lines. The 8-level version of GENIE-1 is shown as a thin solid black line, while the improvement in decadal-scale $CO_2$ uptake resulting from doubling the vertical resolution is illustrated by the thin dashed black line. The bottom plot shows the same data, but plotted on a logarithmic time axis to help visually separate out the different time-scales of $CO_2$ invasion.